

Direct observation of local chemical surface properties by scanning tunneling microscopy

Harry E. Hoster

Citation: [AIP Conf. Proc. 1454](#), 9 (2012); doi: 10.1063/1.4730676

View online: <http://dx.doi.org/10.1063/1.4730676>

View Table of Contents: <http://proceedings.aip.org/dbt/dbt.jsp?KEY=APCPCS&Volume=1454&Issue=1>

Published by the [American Institute of Physics](#).

Additional information on AIP Conf. Proc.

Journal Homepage: <http://proceedings.aip.org/>

Journal Information: http://proceedings.aip.org/about/about_the_proceedings

Top downloads: http://proceedings.aip.org/dbt/most_downloaded.jsp?KEY=APCPCS

Information for Authors: http://proceedings.aip.org/authors/information_for_authors

ADVERTISEMENT



The advertisement features the **AIP Advances** logo, which includes the text "AIP Advances" in a stylized blue and green font, with a series of orange spheres forming a trail above the "A". Below the logo is a green rectangular button with the text "Submit Now" in white.

Explore AIP's new
open-access journal

- Article-level metrics now available
- Join the conversation! Rate & comment on articles

Submit Now

Direct observation of local chemical surface properties by scanning tunneling microscopy

Harry E. Hoster

Technische Universität München, TUM CREATE Centre for Electromobility, Singapore
62 Nanyang Drive, Block 1.2, #01-28, Singapore 637459
harry.hoster@tum-create.edu.sg

Abstract. Vapor deposited Pt films with a thickness locally varying between one and two atomic layers on Ru(0001) are studied as model surfaces with a well-defined lateral variation of the chemical properties. These are probed by reversible CO adsorption at 300 K and with CO pressures in the range $p_{CO}=10^{-10}\dots10^{-5}$ mbar under real-time STM observation. Upon exposure to 10^{-5} mbar CO, no densely packed adlayer is formed on the areas with a local thickness of one atomic layer, whereas a c(4×2) adlayer containing 0.5 CO molecules per surface atom is reversibly formed on areas with locally two atomic layers of Pt. Based on experimental and theoretical data points and parameters from the literature we calculate adsorption isotherms for Pt(111) and the two Ru(0001) supported Pt thin films at 300 K. For all three surfaces, STM observations on CO adsorption are found to be fully consistent with the respective isotherms.

Keywords: Bimetallic Surfaces, Adsorption, Scanning Tunneling Microscopy

PACS: 68.35.bd; 68.37.Ef; 68.43.Fg; 82.45.Jn

INTRODUCTION

The physical properties of solid surfaces are closely entangled with their chemical properties. In combination, both determine the interaction with matter, e.g., in the technologically important fields of heterogeneous catalysis or electrochemistry. Accordingly, the methods of fundamental surface science play a central role in catalysis research since decades [1-3]. Due to its high activity in low temperature fuel cell anodes for the oxidation of CO contaminated H₂ or the direct electrochemical oxidation of methanol the metal combination Pt+Ru continuously was subject of research over the last decades. Apart from the electrochemistry community [4-8], also the Surface Science community was significantly involved [9-20].

Early concepts to explain the enhanced electrocatalytic activity of Pt-Ru mainly refer to a bi-functional Langmuir-Hinshelwood mechanism, where an oxygenated species formed at Ru by H₂O dissociation is acting as co-reactant to remove CO from Pt sites.⁵ As a result of the continuously improved microscopic picture of surface chemistry, however, more recent works put a particular emphasize on the influence of Pt-Ru bonds (ligand

effect) and lattice strain on the local reactivity of Pt and Ru [9, 16-21]. These will affect the coverages of desired (e.g., H) and undesired (e.g., CO) adsorbates and also the rates of associated surfaces reactions [22]. Among the model surfaces studied in the cited works, atomically thin Pt films on Ru(0001) play a distinctive role. Pt was found to grow in atomically smooth, pseudomorphic layers on Ru(0001). Hence, the Pt atoms thus assume the lateral atom-atom distance as in the Ru(0001) plane, which is 0.271 nm as compared to 0.277 nm in the Pt(111) surface. Compared to Pt(111), the Pt films are thus laterally compressed, which according to the d-band model of Hammer and Norskov [23,24] makes CO adsorption weaker. In addition to the lattice compression, the bonds to the underlying Ru atoms further destabilize the interaction of the Pt atoms with surface adsorbates, including CO [9,17,20,23-25]. The latter can be rationalized by a simple bond order argument: Pt is more strongly bound to Ru than to Pt [13], which reduces its bonding power for the interaction with a third species, e.g., an adsorbate. DFT calculations explicitly show for the cases of CO_{ad} [17], H_{ad} [9], O_{ad} [25] that the destabilizing effect of the Pt-Ru bond becomes weaker with increasing Pt layer thickness. For these surfaces, it is possible to work at corresponding systems in experiment and

theory. These structures could be modeled as periodic slabs in density functional theory calculations (DFT), which in turn allowed quantifying the contributions of lattice strain and Pt–Ru heteroatomic bonds, respectively, to the chemical properties of the outermost Pt layer. Up to now, the adsorption energies of CO [17], O [25], and H [9] were calculated as a function of the layer thickness. Direct comparison to experimental data was done by thermal desorption [17,18] and vibrational spectroscopy [18], for CO and by reversible cyclic voltammetry for H [9]. The latter study obviously had a direct relation to the behavior of Pt thin films at the solid|liquid interface and at room temperature. In particular, the cyclic voltammetry experiments are probing equilibrium conditions, i.e., the potential dependent equilibrium H coverage at room temperature. For the CO adlayers, however, no experimental data on the behavior under conditions of an adsorption equilibrium are available so far. The work by Jakob et al [18] is comprehensive in the parameter space of CO coverage and Pt layer thickness but all equilibrated adlayers were studied at a surface temperature of 80 K.

The present paper will make use of fast scanning tunneling microscopy (STM) to directly observe the reversible formation of CO adlayers on Pt–mono and bilayers on Ru(0001) at room temperature (300 K) and at a CO pressure of up to 10^{-5} mbar. This approach is similar to the work by Longwitz et al. [26], who studied CO adlayers on Pt(111) in a pressure range between 10^{-6} and 1 mbar, and to a study by Gsell et al. on the effect of local strain on the adsorption of O at Ru(0001) [27].

After a brief description of the experimental setup and procedures, this paper will report on the real-time STM observation of the CO pressure dependent adlayer formation on Pt mono- and bilayers on Ru(0001). The observations will be compared to previous experimental and theoretic works at the solid|gas interface, including the calculation of CO adsorption isotherms for Pt mono- and bilayers on Ru(0001). Finally, implications of the observed phenomena for the electrocatalytic properties at the solid|liquid interface will be discussed.

EXPERIMENTAL SETUP

The data shown in this work were recorded by a pocket-size STM [28] based in an ultrahigh vacuum (UHV) system (base pressure: $6 \cdot 10^{-11}$ mbar). By means of home-made software and an improved AD/DA interface [29], the STM is capable of scanning up to 25 images per second in constant

height mode. Apart from the STM, the UHV system is equipped with standard facilities for surface preparation and characterization, specifically an electron beam evaporation source (Omicron/Focus EFM 3) for Pt vapour deposition, a cylindrical mirror analyser (Physical Instruments) for Auger electron spectroscopy (AES), and a quadrupole mass spectrometer (Balzers QMS 112) for residual gas analysis. The Ru(0001) single-crystal, which is shaped as a flat ‘hat’, is fixed in a tantalum sample holder with an outer diameter of 18 mm, which is in turn held in a precision sample manipulator that allows for rapid heating (~ 100 K s $^{-1}$) by electron bombardment. Clean Ru(0001) surfaces are prepared by cycles of Ar $^{+}$ ion bombardment (sputtering) and annealing to temperatures > 1100 K, followed by oxygen adsorption/desorption cycles and final annealing to ~ 1750 K to remove residual adsorbed oxygen [16]. The sample temperature is measured by an infrared pyrometer (Impac Infratherm IGA 140). For STM measurements, the sample is transferred from the manipulator to the STM by two wobble sticks. For surface structure analysis, the STM is run in constant current mode, whereas constant height mode is used for fast scanning.

RESULTS AND DISCUSSION

Figure 1a shows the surface morphology after deposition of ~ 1.2 ML (monolayer, 1 ML = one adsorbate or foreign metal atom per surface atom) Pt onto Ru(0001) at room temperature, followed by flash annealing to 800 K. The morphology of the atomically smooth surface is characterized by ribbons of step decorations and hexagonal islands, where the local Pt film thickness is 2 ML. The remaining fraction of the surface is covered by a single Pt monolayer (see also ref. [9]). Close to the buried Ru(0001) step edges it is possible to record STM images of boundaries between regions of 1 ML and 2 ML local Pt coverage at the same level of height. This allows for fast imaging of these regions in constant-height mode. A sequence of 163 STM images was recorded with a frame rate of five images per second, i.e., the overall sequence covers a period of 33 s. The sample temperature was kept constant at 300 K.

Figure 1c shows an atomic resolution STM image out of this sequence, which was recorded at conditions of ultrahigh vacuum (10^{-10} mbar). The 1 ML | 2 ML border is characterized by a line of fourfold hollow sites. This is due to the different stacking of the outermost layer with respect to the two underlying ones.

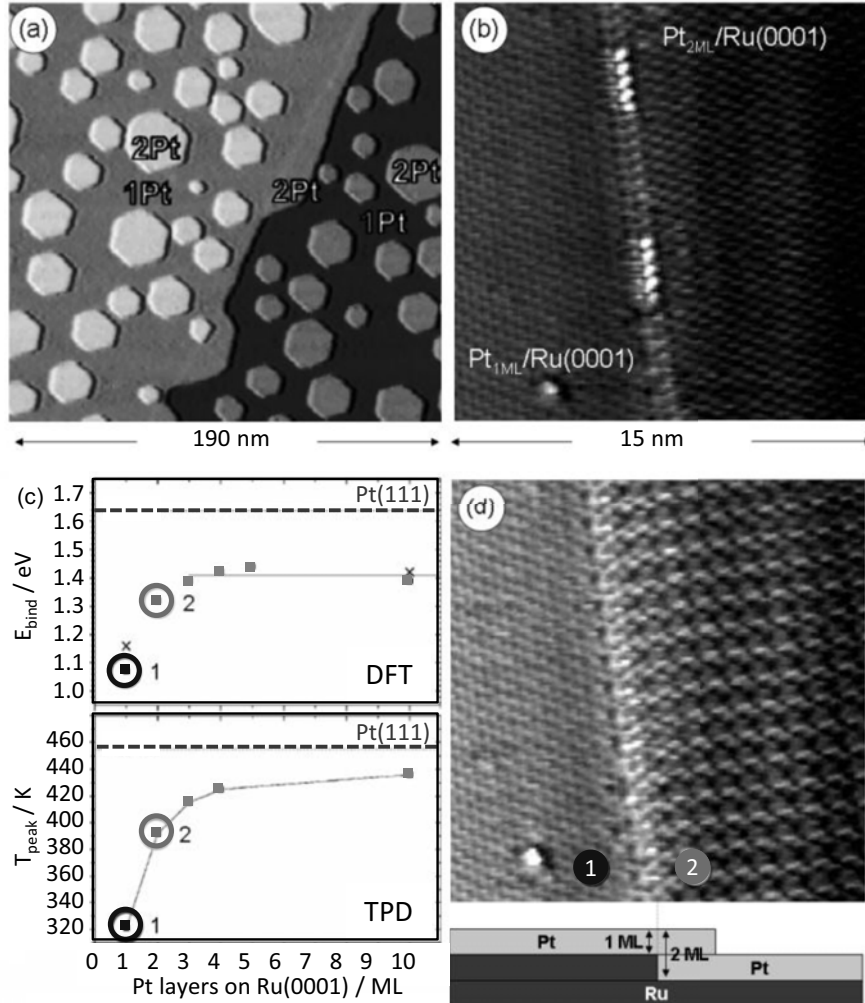


FIGURE 1. Local adsorption properties directly observed by fast STM. (a) STM image of 1.2 ML Pt/Ru(0001) after annealing at 800 K. Regions with 1 ML and 2 ML Pt coexist. (b) Atomically resolved image (recorded with 5 images s^{-1} in constant height mode) of boundary between regions with locally 1 ML and 2 ML Pt. (c) CO adsorption properties of pseudomorphic Pt films with increasing thickness according to ref. [17]. The upper and lower plots show the adsorption energies and desorption peak temperatures, respectively, of CO on Pt films with increasing thickness. (d) Atomically resolved image of the same region as in (b), but at a CO pressure of 10^{-5} mbar. The circles marked 1 and 2 link the surface regions in (d) to the corresponding data points in (c).

Specifically, the first Pt layer adopts to the AB-type stacking of the underlying Ru(0001) layers, whereas the second Pt layer already follows the ABC-type stacking of bulk Pt. This means that the Pt atoms in the 2 ML region and the 1 ML region occupy fcc sites and hcp sites, respectively, which implies the apparent “translational domain boundary” with the rectangular configuration. This assignment is supported by density functional theory calculations which predict AB and ABC stacking for the first and all further Pt layers, respectively [25]. Due to their lower local coordination these fourfold sites should be slightly more attractive for adsorbates than the flat terraces. This fits to the

observation that they are frequently populated by some unidentified bright protrusions during the STM sequence. These protrusions could not be further identified, but they most likely reflect diffusing adsorbates with an increased residence times at the fourfold sites.

Figure 1c summarizes the experimental and calculated findings from ref. [17]. These are the DFT calculated Pt-CO binding energies and peak positions in temperature programmed desorption experiments of CO on Pt mono- and multilayers on Ru(0001) and on Pt(111). Experiments and calculations agree on the prediction that CO adsorption is weakest on

$\text{Pt}_{1\text{ML}}/\text{Ru}(0001)$ becomes stronger with the number of Pt layers. Even for Pt layers films with a thickness of 10 atomic layers, however, CO desorption is shifted to lower temperatures as compared to Pt(111). This can be explained by the pseudomorphic growth of Pt on Ru(0001) that was shown to persists up to $\text{Pt}_{10\text{ML}}/\text{Ru}(0001)$ [30]. The DFT calculations confirm that the compression alone is sufficient to explain the persisting gap in CO stability on $\text{Pt}_{10\text{ML}}/\text{Ru}(0001)$ vs. Pt(111) (data point on the right hand side) [17]. It should be noted that the CO desorption peak for bare Ru(0001) is at around 480 K [31], i.e., the adsorption on that surface is stronger than on Pt(111) or the Ru supported Pt thin films.

According to Figure 1c, the peaks of thermal CO desorption from 1 ML and 2 ML Pt on Ru(0001) are at 320 K and 390 K [17], respectively. For 300 K, this intuitively suggests that CO should be quite unstable on $\text{Pt}_{1\text{ML}}/\text{Ru}(0001)$, whereas on $\text{Pt}_{2\text{ML}}/\text{Ru}(0001)$ it should be possible to adsorb an CO adlayer similar to the one on Pt(111).

When the UHV chamber is backfilled with a CO pressure of 10^{-5} mbar while the sample is kept at 300 K (Figure 1d), the $\text{Pt}_{1\text{ML}}/\text{Ru}(0001)$ region appears largely unaffected, i.e., CO could only be present as mobile adlayer that cannot be imaged by STM. This is different for the $\text{Pt}_{2\text{ML}}/\text{Ru}(0001)$ region on the right hand side of Figure 1d, where a superstructure with a quadratic unit cell becomes visible. This structure is the well-known $c(4\times2)$ phase that is formed on Pt(111) at a CO coverage of 0.5 ML (see Figure 2 for a structure model) [32,33]. The $c(4\times2)$ CO adlayer gives rise to a desorption peak at $T > 450$ K on Pt(111). For $\text{Pt}_{2\text{ML}}/\text{Ru}(0001)$, however, the desorption peak was found to be already at 390 K, with measurable desorption rates even at 300 K [17]. This fits to our observation that the $c(4\times2)$ pattern in Figure 2d disappeared a few minutes after the CO valve was closed and the chamber was pumped down again to UHV conditions.

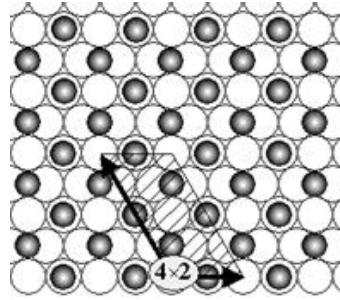


FIGURE 2. Structure model of the $c(4\times2)$ adlayer formed by 0.5 ML CO on Pt(111). Open circles: Pt surface atoms; filled circles: CO molecules.

The observed qualitative similarities suggest that Pt(111) is suitable as reference system to explain the CO adsorption behavior on $\text{Pt}_{1\text{ML}}/\text{Ru}(0001)$ and $\text{Pt}_{2\text{ML}}/\text{Ru}(0001)$ also quantitatively.

In analogy to the previous analysis of the potential dependent H adsorption isotherms on these surfaces [9], where the isotherm for Pt(111) in combination with the DFT results was found sufficient to predict the isotherms for Pt, we will now attempt to predict the pressure dependent CO adsorption isotherms on $\text{Pt}_{1\text{ML}}/\text{Ru}(0001)$ and $\text{Pt}_{2\text{ML}}/\text{Ru}(0001)$. As reference isotherm, we have chosen thermal He scattering data published by Poelsema et al. for Pt(111) at varied CO pressure [34]. The same study also served as key reference point in a recent comprehensive computational treatment of CO on Pt(111) [32]. Poelsema et al. found that CO adsorption on Pt(111) at coverages $\theta_{\text{CO}} < 0.1$ ML can be fitted by a Frumkin (= Fowler-Guggenheim) isotherm of the form

$$p_{\text{CO}} = \frac{\theta_{\text{CO}}}{1 - \theta_{\text{CO}}} K T^3 \exp\left(-\frac{E_{d,\text{Pt}(111),\theta_{\text{CO}}=0} + \varepsilon \theta_{\text{CO}}}{k_B T}\right)$$

θ_{CO} = CO coverage

p = CO pressure

T = surface temperature

$k_B = 8.617 \cdot 10^{-5} \text{ eV K}^{-1}$ (Boltzmann constant)

$K = 12.5 \text{ mbar K}^{-3}$ = constant

$E_{d,\text{Pt}(111),\theta_{\text{CO}}=0} = 1.378 \text{ eV}$

= desorption barrier of CO on Pt(111)

at $\theta_{\text{CO}} = 0$

$\varepsilon = 0.71 \text{ eV}$ = mean field repulsive interactions

In the cited work, a good data fit at $T=402$ K, 415 K, 427 K, 440 K, and 452 K was obtained with the coverage and temperature independent value of K as shown above. Likewise, also the constant ε was found to be independent of θ_{CO} and T . Figure 3 shows the isotherm for 402 K. For $\theta_{\text{CO}} < 0.17$ ML the curve is drawn as solid line. For higher coverages, the cited work did not explicitly confirm the isotherm by experimental values, which is why this part is considered an extrapolation and therefore drawn as dotted line. For CO on Pt(111), adsorption at 300 K has only been studied for $\theta_{\text{CO}} > 0.5$ ML [26]. Only the high-coverage structures formed in this regime imply sufficiently large desorption rates to establish adsorption equilibrium in reasonable time at that temperature. The coverages were determined from STM images recorded at CO pressures in the range $p_{\text{CO}} = 10^{-8} \dots 10^3$ mbar, see the small circles in Figure 3 for the data points from ref. [26]. Based on the Frumkin isotherm and the parameters listed above, we propose a hypothetic isotherm for CO on Pt(111) at 300 K, plotted as dashed line in Figure 3.

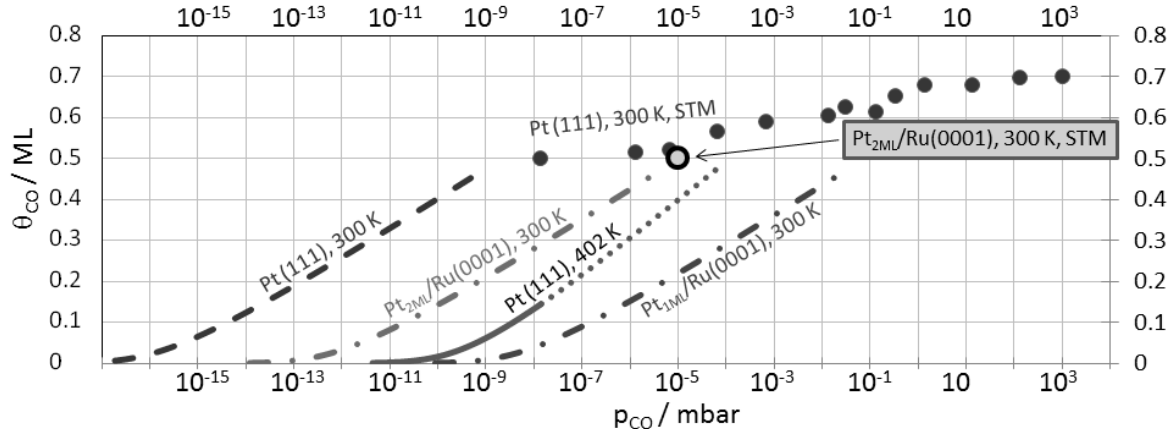


FIGURE 3. Adsorption isotherms of CO on Pt(111), Pt_{1ML}/Ru(0001) and Pt_{2ML}/Ru(0001). For Pt(111), experimental data points were taken from ref. [26] (STM data, small circles) and ref. [34] (solid line). The isotherm for Pt(111) at 402 K is experimentally validated up to 0.17 ML CO, beyond that coverage it is extrapolated (dotted line, see text). The dashed line is the hypothetic isotherm for CO on Pt(111) at 300 K. The dash dotted lines are calculated isotherms based on the experiments in ref. [34] and the adsorption energies of CO on Pt_{1ML}/Ru(0001) and Pt_{2ML}/Ru(0001) from ref. [17]. Large circle: c(4×2) adlayer on Pt_{2ML}/Ru(0001) at 300 K.

According to this plot, CO pressures of $p_{CO} < 10^{-9}$ mbar would have to be established and controlled to attain equilibrium coverages of $\theta_{CO} < 0.5$ ML. Reliable measurements of CO equilibrium coverages in this pressure regime would be very difficult due to the influence of the rest gas and the slow adsorption/desorption rates.

Nevertheless, the hypothetic isotherm is virtually pointing to the point at the low-coverage limit of the STM study at 300 K, which indicates that it is not too far from the reality.

Based on the DFT results for the CO binding energy on Pt(111), Pt_{1ML}/Ru(0001), and Pt_{2ML}/Ru(0001) (see Figure 1c), we have calculated the isotherms for CO on Pt_{1ML}/Ru(0001) and Pt_{2ML}/Ru(0001) that are plotted as dash-dotted lines in Figure 3. The curves were calculating by using $E_{d,Pt_{1ML}/Ru(0001),\theta_{CO}=0} = 0.928 \text{ eV}$ and $E_{d,Pt_{2ML}/Ru(0001),\theta_{CO}=0} = 1.158 \text{ eV}$ instead of $E_{d,Pt(111),\theta_{CO}=0} = 1.378 \text{ eV}$. The two values for the energy barriers were directly calculated from the experimentally found value for Pt(111) [34] and the differences of the binding energies as obtained by DFT, i.e. 0.45 eV and 0.22 eV for Pt_{1ML}/Ru(0001) and Pt_{2ML}/Ru(0001), respectively. The absolute values of the DFT calculated binding energies, however, were not considered for calculating the curves. All other parameters in the isotherm were kept at the values found for Pt(111). This is similar to the treatment of H adsorption on the same surfaces [9], where the potential dependent H coverages were successfully predicted by just varying the adsorption energies according to corresponding DFT results.

The two isotherms predicted by this DFT based extrapolation are in full agreement with our experimental findings:

1. The CO coverage for Pt_{1ML}/Ru(0001) at $p_{CO}=10^{-5}$ mbar would be $\theta_{CO} \sim 0.25$ ML. A CO adlayer with $\theta_{CO} < 0.33$ ML can be expected to be too mobile for STM imaging at 300 K on any of the Pt surfaces discussed here. This assumption is justified by the known low lateral corrugation of the CO adsorption energy on Pt(111) [32], which should be even lower on Pt_{1ML}/Ru(0001) or Pt_{2ML}/Ru(0001), thus making an STM observation of low CO coverages at 300 K even less likely. Hence, the fact that no evidence for CO is visible on the Pt_{1ML}/Ru(0001) surface is fully consistent with the isotherm.
2. According to Figure 3, the isotherm for adsorption on Pt_{2ML}/Ru(0001) at 300 K would predict a CO coverage of 0.5 ML at $p_{CO}=10^{-5}$ mbar, in perfect agreement with the STM observation (see Figure 5b). Furthermore, the fact that the c(4×2) pattern disappears when the CO supply is stopped confirms that it indeed belongs to a reversibly adsorbed adlayer in equilibrium with the gas phase.

CONCLUSIONS

Pt films with a thickness of one atomic layer on Ru(0001) behave rather inert in their interaction with CO. Complementarily to previous thermal desorption and vibrational spectroscopy experiments, this was now shown by fast scanning STM during exposure to CO at 300 K. No CO related features became visible in

the STM images, indicative for a coverage < 0.33 ML, but rather much lower.

On Pt films with a thickness of two atomic layers on Ru(0001), however, an exposure to 10^{-5} mbar CO at 300 K leads to the formation of a $c(4\times 2)$ adlayer with a coverage of 0.5 ML. The adlayer disappears when the surface is exposed to vacuum again. The same adlayer is known to form on Pt(111) where it remains stable at 300 K even without continuous CO exposure. We have shown that our observations could have been predicted by combining (i) the adsorption isotherm of Pt(111) for $T = 402$ K and (ii) the difference of the CO binding energies on Pt(111) and on the Pt bilayer on Ru(0001) as determined by DFT. This underlines the capability of DFT to correctly predict the adsorption properties of tuned bimetallic surfaces when proper reference systems are taken into consideration.

ACKNOWLEDGMENTS

The STM data shown in this work were recorded at the Institute of Surface Chemistry and Catalysis at Ulm University. Fruitful discussions with T. Hager, H. Rauscher, and R.J. Behm are gratefully acknowledged.

REFERENCES

1. G.A. Somorjai and J.Y. Park, *Surface Science* **603**, 1293–1300 (2009).
2. C.T. Campbell, in *Handbook of Heterogeneous Catalysis*, edited by G. Ertl, H. Knözinger, and J. Weitkamp, Weinheim: Wiley-VCH, 1997, pp. 814–826.
3. G.A. Somorjai, *Journal of Physical Chemistry* **94**, 1013–1023 (1990).
4. O. Petry, B. Podlovchenko, A. Frumkin, and H. Lal, *Journal of Electroanalytical Chemistry* (1959) **10**, 253–269 (1965).
5. M. Watanabe and S. Motoo, *Journal of Electroanalytical Chemistry* **60**, 275–283 (1975).
6. H.A. Gasteiger, N.M. Markovic, and P.N. Ross, *Journal of Physical Chemistry* **99**, 16757–16767 (1995).
7. H.A. Gasteiger, N. Markovic, P.N. Ross, and E.J. Cairns, *Journal of Physical Chemistry* **98**, 617–625 (1994).
8. Y. Shimodaira, T. Tanaka, T. Miura, A. Kudo, and H. Kobayashi, *Journal of Physical Chemistry C* **111**, 272–279 (2007).
9. H.E. Hoster, O.B. Alves, and M.T.M. Koper, *Chem. Phys. Chem.* **11**, 1518–1524 (2010).
10. J.C. Davies, B.E. Hayden, and D.J. Pegg, *Electrochimica Acta* **44**, 1181–1190 (1998).
11. H.E. Hoster, T. Iwasita, H. Baumgärtner, and W. Vielstich, *Phys. Chem. Chem. Phys.* **3**, 337–346 (2001).
12. H.E. Hoster and H.A. Gasteiger, in *Handbook of Fuel Cells - Fundamentals Technology and Applications*, edited by W. Vielstich, H.A. Gasteiger, and A. Lamm, Chichester: Wiley, 2003, pp. 236–265.
13. A. Bergbreiter, A. Berko, P.M. Erne, H.E. Hoster, and R.J. Behm, *Vacuum* **84**, 13 – 18 (2009).
14. A. Bergbreiter, H.E. Hoster, and R.J. Behm, *Chem. Phys. Chem.* **12**, 1148–1154 (2011).
15. H. Hoster, A. Bergbreiter, P. Erne, T. Hager, H. Rauscher, and R. Behm, *Phys. Chem. Chem. Phys.* **10**, 3812–3823 (2008).
16. F. Buatier de Mongeot, M. Scherer, B. Gleich, E. Kopatzki, and R. Behm, *Surface Science* **411**, 249–262 (1998).
17. A. Schlapka, M. Lischka, A. Groß, U. Käsberger, and P. Jakob, *Physical Review Letters* **91**, 016101 (2003).
18. P. Jakob and A. Schlapka, *Surface Science* **601**, 3556–3568 (2007).
19. H. Rauscher, T. Hager, T. Diermant, H. Hoster, F. Buatier de Mongeot, and R.J. Behm, *Surface Science* **601**, 4608–4619 (2007).
20. H.E. Hoster, M.J. Janik, M. Neurock, and R.J. Behm, *Physical Chemistry Chemical Physics* **12**, 10388–10397 (2010).
21. H.E. Hoster and R.J. Behm, in *Fuel Cell Catalysis: A Surface Science Approach*, edited by M.T.M. Koper, Chichester: Wiley&Sons, 2008, pp. 465–505.
22. T. Bligaard, J.K. Nørskov, S. Dahl, J. Matthiesen, C.H. Christensen, and J. Sehested, *Journal of Catalysis* **224**, 206–217 (2004).
23. M. Mavrikakis, B. Hammer, and J.K. Nørskov, *Physical Review Letters* **81**, 2819–2822 (1998).
24. B. Hammer and J. Nørskov, *Surface Science* **343**, 211–220 (1995).
25. M. Lischka, C. Mosch, and A. Gross, *Electrochimica Acta* **52**, 2219 (2007).
26. S.R. Longwitz, J. Schnadt, E.K. Vestergaard, R.T. Vang, I. Stensgaard, H. Brune, and F. Besenbacher, *The Journal of Physical Chemistry B* **108**, 14497–14502 (2004).
27. M. Gsell, P. Jakob, and D. Menzel, *Science* **280**, 1–4 (1998).
28. K.E. Kopatzki, *Sauerstoffadsorption, Oxidbildung Und Homoepitaxie Auf Ni(100) Oberflächen - Eine Untersuchung Mit Dem Rastertunnelmikroskop*, Ludwig-Maximilians Universität München, 1994.
29. L. Zitzler, B. Gleich, O.M. Magnussen, and R.J. Behm, in *Localized In Situ Methods for Investigating Electrochemical Interfaces*, Eds. A.C. Hillier, M. Seo, S.R. Taylor, Proc. Electrochem. Soc., 99–28, 2000, pp. 29–38.
30. P. Jakob and A. Schlapka, *Surface Science* **601**, 3556–3568 (2007).
31. H. Pfür, P. Feulner, and D. Menzel, *Journal of Chemical Physics* **79**, 4613–4623 (1983).
32. J.S. McEwen, S. Payne, H. Kreuzer, M. Kinne, R. Denecke, and H.P. Steinrück, *Surface Science* **545**, 47–69 (2003).
33. G. Ertl, M. Neumann, and K. Streit, *Surface Science* **64**, 393–410 (1977).
34. B. Poelsema, R.L. Palmer, and G. Comsa, *Surface Science* **136**, 1–14 (1984).